Available online at www.sciencedirect.com
ScienceDirect
Trans. Nonferrous Met. Soc. China 30(2020) 1756−1770
Transactions of Nonferrous Metals Society of China
www.tnmsc.cn

Microstructural characterization and mechanical properties of friction surfaced AA2024−Ag composites

Parisa PIRHAYATI, Hamed JAMSHIDI AVAL

Department of Materials Engineering, Babol Noshirvani University of Technology, Shariati Avenue, Babol 47148-71167, Iran

Received 23 November 2019; accepted 21 May 2020

Abstract: The effects of Ag on the microstructure, mechanical properties, and electrical conductivity of AA2024 aluminum alloy coating were investigated. It was fabricated by friction surfacing as an additive manufacturing process. To carry out this investigation, Ag was added by 5.3, 10.6, and 16.0 wt.% to an AA2024 consumable rod by inserting holes in it. It was found that due to the strengthening by solid solution and the formation of precipitates and intermetallic containing Ag, the driving force for grain growth is reduced and consequently the grain size of the coating is decreased. After artificial aging heat treatment, the electrical conductivities of the coatings containing 0 and 16.0 wt.% Ag are increased by 4.15% (IACS) and decreased by 2.15% (IACS), respectively. While considering a linear relationship, it can be proposed that for a 1 wt.% Ag increase, the strength and hardness of the coating will be increased by 1.8% and 1.0%, respectively. It was established that the effect of $Al_6(Cu,Ag)Mg_4$ precipitate formation on strengthening is greater than that of Ag-rich intermetallic.

Key words: friction surfacing; AA2024 aluminum alloy; Ag powder; AA2024−Ag composite

1 Introduction

Copper and aluminum have been currently the most widely used metals in electronics and electrical engineering. Although mechanical strength and electrical conductivity are inverse properties where their equilibrium can be considered as one of the engineering touch challenges in conducting material design, the simultaneous existence of these properties is, in fact, the main purpose. Pure copper and aluminum possess low mechanical strength. In general, pure materials can be strengthened by adding barriers to their dislocation motion [1]. Moreover, there are three well-known methods for alloy reinforcement, namely, the solid solution hardening, precipitation hardening, and work hardening. An appropriate method to strengthen the alloy without a drastic loss in the electrical conductivity is to combine all three methods, i.e., the work hardening, solid solution hardening, and the precipitation hardening [2].

Although aluminum is more intrinsically electrically resistant in comparison to copper, due to its lower density and price than copper, the general impetus for the development of high strength conductors made of aluminum and its alloys has drastically increased. According to the equilibrium phase diagram, in terms of solubility in the aluminum matrix, the metal elements are divided into two major categories with a low level of solubility such as nickel, titanium, tungsten and copper, and a high level of solubility such as zinc and silver. The use of high soluble elements in aluminum alloys can greatly alter the chemical composition of the aluminum. For instance, if the requirements of the precipitation hardening process are fully provided, the precipitation hardening

Corresponding author: Hamed JAMSHIDI AVAL; Tel: +98-11-35501808; Fax: +98-11-35501802; E-mail: h.jamshidi@nit.ac.ir
DOI: 10.1016/S1003-6326(20)65336-5

mechanism occurs. Moreover, silver has a high level of solubility in aluminum, about 55.6 wt.% at 570 °C while its solubility decreases a negligible amount at room temperature. The silver-containing 2000-series aluminum alloys have been used more widely and developed as high-strength materials in recent years compared to conventional alloys such as AA2219 and AA2618 [3−6]. Generally speaking, silver-containing alloys, although rather expensive, are more desirable, mainly due to their higher strength and thermal stability. The advantages that these alloys present over the other 2000-series aluminum alloys are partly due to the amount of produced precipitates during their artificial aging. According to the research by AULD et al [7], adding 0.5 wt.% Ag to Al−Cu−Mg alloy with a Cu/Mg mass ratio of 1.66:1 results in an increase in the aging kinetic, as well as the maximum hardness in the 120−240 °C temperature range. Furthermore, examination of the precipitation process in this alloy revealed that this process consists of two stages, namely, the first step is the high-speed hardening and the formation of GPB zones, while the second step is the increase in hardness associated with the formation of *T* precipitates as temperature rises. It should be noted that once the *S* precipitates form, the alloy begins to soften again in the second step. Several studies have indicated that the composition of *T* precipitates is quite close to $Al_6(Cu,Ag)Mg_4$. As the research continues, it is observed that in the Al−Cu−Mg system with a Cu/Mg mass ratio of 1:0.4−1:2.1, silver encourages the formation of FCC precipitates with the composition of $Al_6(Cu,Ag)Mg_4$ alongside of *S* (Al_2CuMg) precipitates [8−10]. On the other hand, in the Al−Cu−Mg alloy system with a Cu/Mg mass ratio of 1:5, *T* precipitates are not formed while θ ($CuAl_2$) precipitates are formed. However, the precipitates are formed with the same chemical composition on the {111} aluminum surfaces in the presence of silver due to the difference with the conventional Al−Cu system in which the θ ($CuAl_2$) precipitates are formed on {100} surfaces. These precipitates, formed on the {111} surfaces, are referred to as Ω precipitates. Numerous studies have proposed that the greatest impact of silver on the precipitation behavior of the Al−Cu−Mg alloy system occurs when the Cu/Mg mass ratio is approximately 1:10 and the copper content is between 5 and 6 wt.% [11].

The fabrication of layered metallic composites and the use of materials possessing different mechanical and electrical properties are a number of areas of interest in various researches [12−20]. Friction surfacing as an additive manufacturing process is a rather new method based on solid-state welding processes, whereby similar and dissimilar metals can be coated much more effectively on a substrate compared to other similar processes. Moreover, the friction surfacing process is primarily centered on the plastic deformation of the consumable rod. In this process, the consumable material is rotated at a constant velocity, affected by the axial force on the substrate which leads to the generation of frictional heat at the interface of the substrate and rod. Consequently, the frictional heat produces a viscoplastic layer at the tip of the rod where due to the temperature and pressure, a metal bond is created between the deformed material and the substrate. Based on the available resources, the friction surfacing process is mainly known and utilized as a coating method [21,22]. However, because of the nature of the process and the severe plastic deformation associated with the heat generation, this process is capable of modifying and also improving surface properties through changes in the microstructure and chemical composition.

Most of the previous studies on the effects of adding silver to aluminum were carried out in a fashion where silver was added to the aluminum at the liquid state and subsequently, the resulting alloy was investigated in terms of microstructures and mechanical properties. However, it should be duly noted that processes with severe plastic deformation can be used for mechanical alloying [23−26]. As a recent research in the field of adding silver at solid-state and the study of mechanical alloying, PIRHAYATI and JAMSHIDI AVAL [27] studied the effects of silver powder addition on non-isothermal aging of friction surfaced AA2024 aluminum alloy. It was revealed that the AA2024−Ag friction surfaced composite, after solid solution heat treatment, can, in fact, alter the precipitation process of coatings during non-isothermal aging treatment and further improve the mechanical properties. It should also be noted that due to the specificity of the friction surfacing process, it can be utilized as an additive manufacturing method [28−30] in the manufacturing of layered composites and bimetals. In this study, the effects of

adding different amounts of silver to the AA2024 alloy were investigated in terms of the mechanical properties and electrical conductivity of a 2-layerd composite formed by the friction surfacing process. Given the growing status of aluminum and its increasing use in the electronics, it appears that composite fabrication possessing a gradient structure and electrical properties while using solid-state methods can be highly valuable.

2 Experimental

In this research, AA2024 aluminum alloy sheet with a thickness of 2 mm was used as a substrate and AA2024 rod with a diameter of 20 mm was used as mechtrode. The chemical compositions of the substrate and mechtrode are listed in Table 1. Moreover, silver powder with a particle size in the range of 2−10 μm was utilized as an additive to the rod. The SEM image of the silver powder is shown in Fig. 1. The silver powder was then applied to the holes embedded in the cross-section of the rods in order to investigate the effects of addition of silver powder to the coating. As shown in Fig. 2, three different designs of one, two, and three holes were created on the cross-section of the rods. The holes have a diameter of 2.5 mm and a depth of 80 mm. In all of the three designs, the center of the hole is 3 mm away from the center of the rod. In the two-hole design, the holes are at an angle of 180° with respect to each other while the relative angle is 120° in the three-hole design. After drilling, the rods were rinsed thoroughly with ethanol and the initial mass of each sample was carefully measured with a digital scale. The rods were then filled with silver powder and weighed once again where the values of 5.3, 10.6, and 16.0 wt.% were accepted, respectively, for each of the samples according to the number of holes in them after the preparation of consumable rods. The coating process was performed meticulously using axial feeding rate, traverse speed, and rotational speed of 200 mm/min, 125 mm/min, and 600 r/min, respectively using both types of rods containing silver powder or without silver powder. Furthermore, the friction surfacing parameters mentioned here were selected after performing friction surfacing with various axial feeding rates, traverse speeds, and rotational speeds in the ranges of 100−300 mm/min, 75−125 mm/min, and 600−1000 r/min, respectively. The friction surfacing parameters were chosen in order to obtain the highest coating efficiency. Having finished with the friction surfacing, the coated samples were then subjected to homogenization, solid solution (at 540 °C for 4 h), and artificially aging (at 185 °C for 4 h) treatments. The solid solution and aging temperatures and time

Table 1 Chemical compositions of alloys (wt.%)

Alloy	Si	Fe	Cu	Mn	Mg	Al
AA2024 consumable rod	0.22	0.27	3.80	0.51	1.45	Bal.
AA2024 substrate	0.18	0.25	3.21	0.40	1.35	Bal.

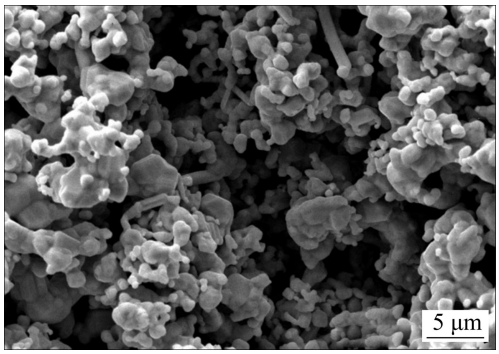

Fig. 1 SEM image of Ag powder

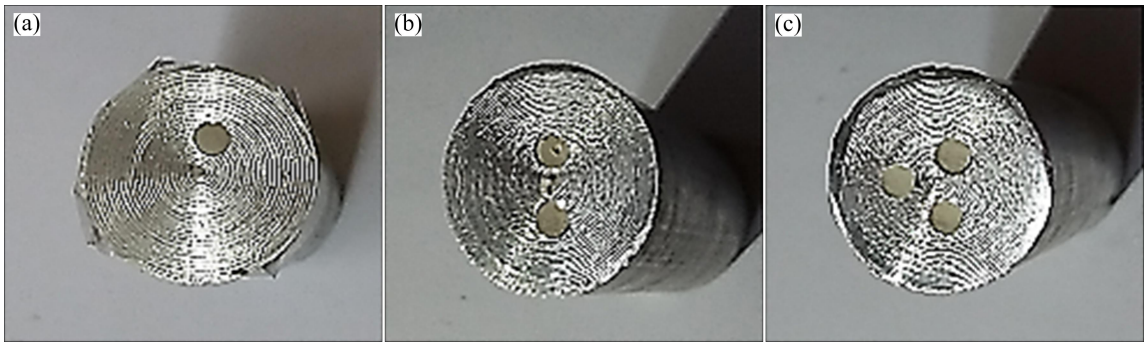

Fig. 2 Three different designs of one (a), two (b) and three (c) holes created on cross-sections of consumable rods

were selected according to repeated experiments to achieve the maximum homogenization and prevent the abnormal grain growth.

For the next step, the microstructures of coated samples were evaluated using metallographic procedures before and after the heat treatment. The metallographic samples of the rod, substrate, and coated samples were first polished with 60−3000 grit SiC paper and then their surfaces were completely cleaned with ethanol. Subsequently, the samples were polished using an alumina solution and etched by a Keller's reagent. The optical microscope (DG Victory−Dewinter) and FEI ESEM QUANTA 200 scanning electron microscope equipped with X-ray diffraction EDS were used to study the microstructure. As shown in Fig. 3, in order to evaluate the microstructure homogeneity, the microstructural examination of the coating was performed in four zones including the interface, advancing side, center, and retreating side of the coating. X-ray diffraction (XRD) tests were incorporated to identify the phases in the microstructure. Moreover, XRD analysis was performed using the XRD Rigaku Ultima IV. Shear punch and hardness tests were also carried out to investigate the mechanical properties of the coatings. Shear punch test was performed according to the method described in Ref. [31]. The Brinell hardness was measured using a Koopa UV1 hardness tester in accordance with ASTM E10 standard with a load of 15 kg and a dwell time of 10 s in order to measure the exact hardness of the coatings. The electrical conductivity of coatings was also calculated with a model 4200−SCS semiconductor characterization system (SCS).

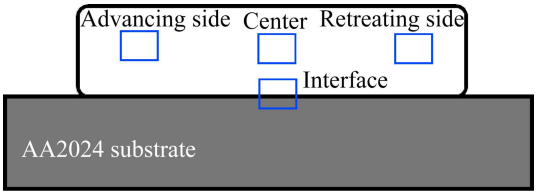

Fig. 3 Selected zones for investigation of microstructure

3 Results and discussion

Figure 4 illustrates the cross-sections of silver-containing and silver-free coated samples. During the friction surfacing process, the materials in the consumable rod are affected by a thermo-mechanical process (severe plastic deformation and exposure to heat). The friction surfacing process is fully capable of producing a continuous coating under friction and a continuous plastic deformation of the rod. The values for coating efficiency ($\eta_{coating}$) were calculated according to Eq. (1) [21] while using different samples. The obtained results are reported in Table 2.

$$\eta_{coating} = \frac{W_a}{W_b}\frac{AV}{\pi r^2 S} \quad (1)$$

where W_a and W_b are the bonded and maximum coating widths, respectively, A is the area of the coating cross-section (determined by multiplying the width and height of the coating layer), S is the traverse velocity, V is the axial feeding rate, and r is the radius of the mechtrode.

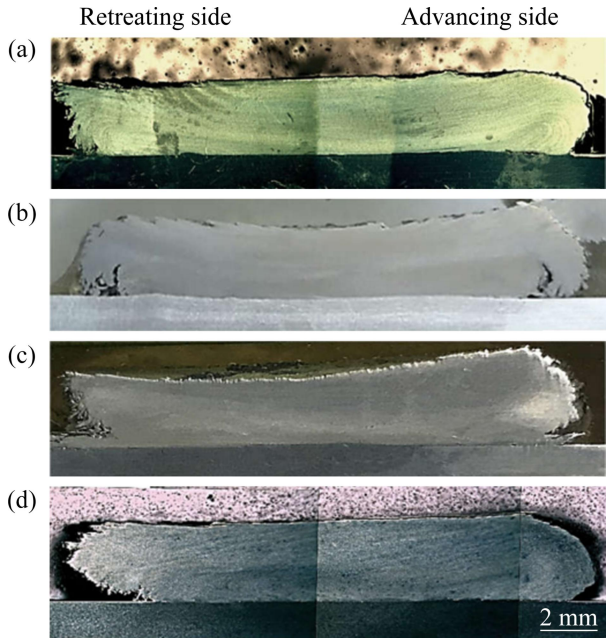

Fig. 4 Cross-sections of coated samples containing different contents of Ag: (a) 0 wt.%; (b) 5.3 wt.%; (c) 10.6 wt.%; (d) 16.0 wt.%

Table 2 Coating efficiencies for various samples

Ag content/wt.%	0	5.3	10.6	16.0
Coating efficiency/%	20.01	19.68	19.32	18.85

As one can observe, a reduction in the coating efficiency can be initiated by the addition of a minor amount of Ag powder in a manner where the coating efficiency decreases up to 1.16% as the Ag amount increases to 16.0 wt.%. It is rather clear that the frictional behavior of the rod with Ag is different from the Ag-free rod since a difference

exists between the additive and metallic matrixes. Therefore, the difference between the heat input and plastic deformation regarding the Ag-containing consumable rod and the Ag-free rod is reasonable. This probably results in a lower level of coating efficiency associated with the rod having Ag powder.

The microstructures of AA2024 as the consumable rod, the substrate and the coatings with and without Ag are shown in Fig. 5. Moreover, at the consumable rod cross-section, the mean grain size is equal to 150 μm. Based on the arrangement of grains stretching in the longitudinal direction equivalent of the extrusion direction, the length and width of the microstructure grains were measured to be 1000 and 150 μm, respectively. It should also be mentioned that before applying the heat treatment, the mean constituent sizes of the rod and substrate were equal to (8.1±1.2) and (5.1±1.1) μm, respectively. There are two possibilities regarding the rod and substrate microstructures while taking into account the EDS analysis. Firstly, these microstructures have Fe-rich particles, and secondly, they possess chemical compositions close to $CuAl_2$ and Al_2CuMg.

Before applying the heat treatment, the mean grain sizes in the midpoint of coatings with Ag contents of 5.3, 10.6, 16.0 wt.% and Ag-free were equal to (12.21±0.95), (11.71±1.08), (11.13±1.12), and (13.91±1.42) μm, respectively. Furthermore, the formation of fine grains in a coating manufactured by the friction surfacing process should be considered as a significant fact. As previously mentioned, this was probably due to the severe plastic deformation as well as the heat applied through the process of coating which led to dynamic recrystallization [32]. Based on the previous observations, the dynamic recrystallization occurred in both Ag-containing and Ag-free coatings; however, the grain size is finer in the former than that in the latter. Although the difference between the grain sizes of the coated samples is rather insignificant, it may need further investigation. Given the research conducted by MUZYK et al [33], the stacking fault energy (SFE) of the aluminum matrix was not greatly influenced by adding Ag to Al. Hence, it can be concluded that the mechanism associated with the dynamic recrystallization is not dependent on the presence of Ag in the coating. On the other hand, the finer grains present in the Ag-containing sample can have various explanations, e.g., the high solubility of Ag in Al. Moreover, Ag can easily diffuse and then dissolve in Al because of the high temperature and severe plastic deformation existing in the coating process. It is worthy to note that several diffusion paths are created by the severe plastic deformation in addition to the high density of dislocations [34]. For that very reason, adding a solid solution and a Ag-containing intermetallic compound can lead to a decrease in the driving force of the grain growth. Subsequently, the coating grain size is reduced. Regardless of the parameters important in this process, the plastic strain and deformation behavior related to the coating can be affected by the holes drilled on the cross-section of the Ag-containing rod. In addition, the coating grain size can also be influenced by the formation of the Al−Ag solid solution.

As shown in Fig. 5, as a general rule, regardless of the amount of Ag present in any coating, the microstructures on the advancing and retreating sides are not different from those in the center. In other words, due to the high thermal conductivity of Al and the rapid heat transfer to the surrounding environment, a significant difference cannot be observed in the overall microstructure. The microstructure of the coating/substrate interface shows a defect-free joint on the coatings. However, the sought-after process is the formation of a gradient microstructure in the coatings. As mentioned earlier, the occurrence of dynamic recrystallization can cause this type of gradient structure to fully form. It should be noted that the microstructure at the coating/substrate interface is finer in comparison with that of the upper region of the coating due to the more rapid heat transfer to the substrate [35,36]. Furthermore, as can be seen in Fig. 5, close to the interface region and on the advancing side of the samples with 5.3 and 10.6 wt.% Ag, agglomeration of Ag can be observed. The occurrence of this phenomenon can be fully explained by the fact that the holes design in the Ag-containing samples is expected to change the distribution of the Ag powder in the coating.

Figure 6 shows the comparison made based on the XRD results in relation to the two coatings with and without Ag before applying heat treatment. In a similar fashion and based on the same analysis, the diffraction angle of Al with the maximum intensity

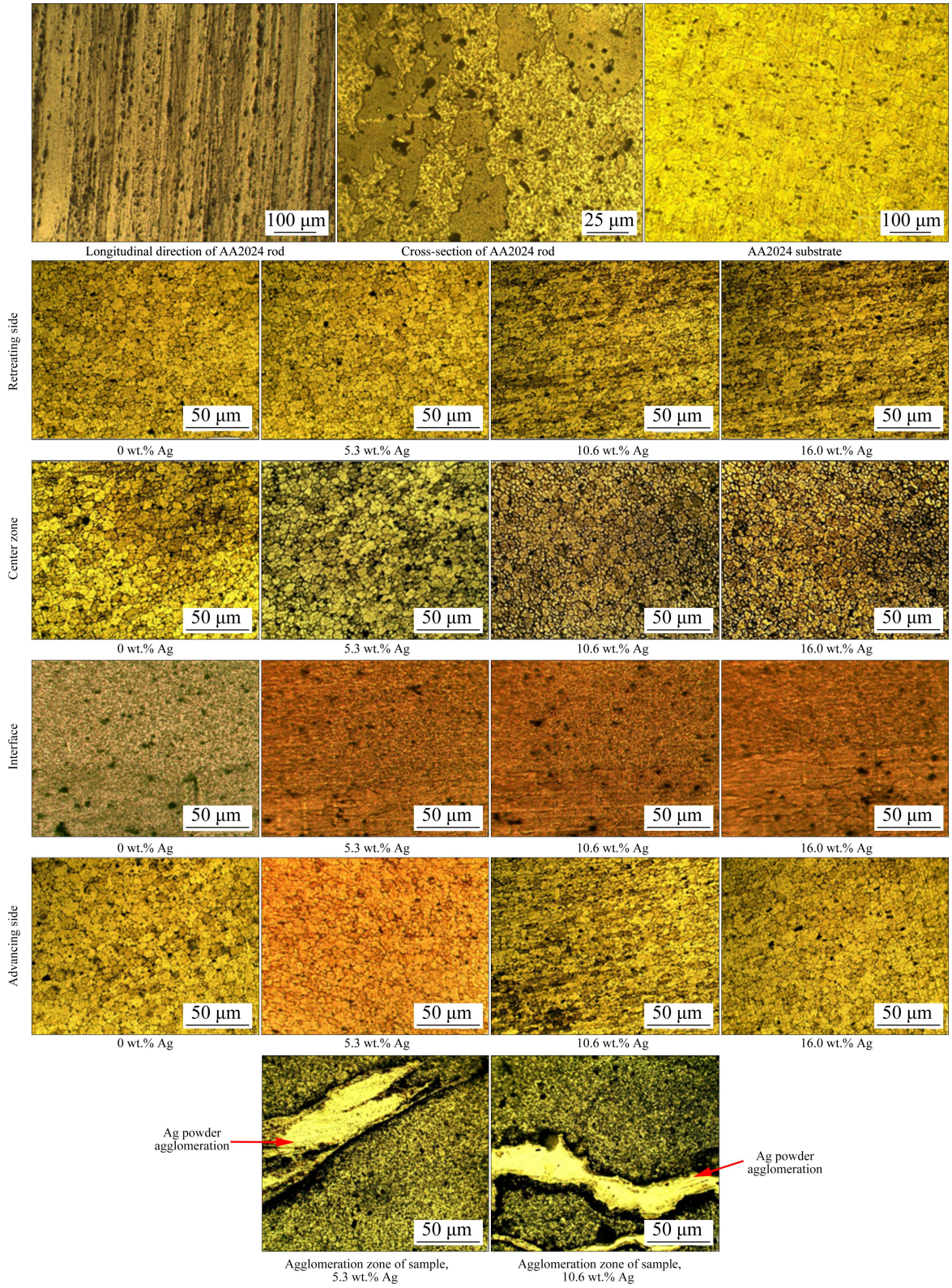

Fig. 5 Microstructures of consumable rod, substrate and different zones of coated samples

is presented in Table 3. It can be observed that a Ag-containing coated sample has lower angles compared to the coated sample without Ag. This then leads to an upsurge in the unit cell parameter of the Al matrix. It should also be mentioned that the aforementioned parameter was obtained using an extrapolation approach carried out by NELSON and RILEY [37]. The atomic radius of Ag (1.44 Å) is slightly greater than that of Al (1.43 Å). Thus, it can be predicted that by substituting the Al atoms

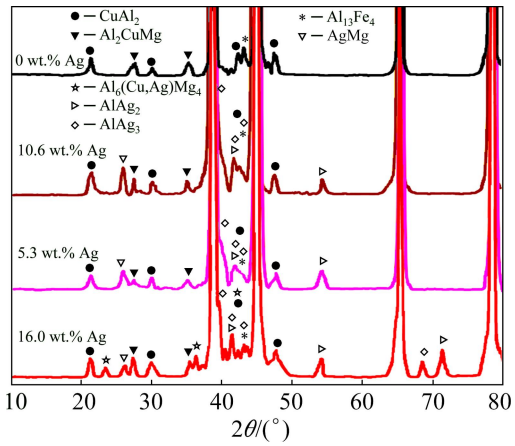

Fig. 6 XRD patterns of coated samples before heat treatment

Table 3 Diffraction angles of Al peak with maximum intensity at different contents of Ag

Ag content/wt.%	0	5.3	10.6	16.0
Diffraction angle/(°)	36.72	36.71	36.69	36.65

with Ag ones in the aluminum structure, an enhancement in the lattice parameter of the Al−Ag solid solution can be obtained. As a result, the formation of solid solution can be attributed to this lattice parameter enhancement after the application of friction surfacing process to the Ag-containing coating. The holes drilled in the consumable rod, which are able to alter the friction condition and subsequently decrease the frictional heat in the coating process, are known as the other main reason for the formation of solid solution. Thus, the lower the heat during the process is, the slower the grain growth in the Ag-containing coating samples is. Nevertheless, in the Ag-free coating samples, we encountered a higher level of heat generation due to the constant cross-section of the rod as well as steady friction conditions in the period of friction surfacing process. Based on the X-ray diffraction results, different phases including Al_2CuMg, $CuAl_2$, and $Al_{13}Fe_4$ are formed in both Ag-containing and Ag-free coating samples before applying the heat treatment. Moreover, other phases such as $AlAg_2$, $AlAg_3$, and AgMg are present in the coating samples containing Ag powder. It is worth noting that the $Al_6(Cu,Ag)Mg_4$ precipitates can be observed solely in the coating with 16.0 wt.% Ag. The Al_6CuMg_4 precipitates, according to the Al−Cu−Mg phase diagram, are low-temperature precipitates, which tend to form at low temperatures yet dissolve at high temperatures. Furthermore, the strength of Al_6CuMg_4 precipitates is enhanced by the addition of micro-alloy elements such as Ag. The diffusion coefficients of Ag and Cu in the aluminum matrix are 5.7 and 0.14, respectively [38]. Due to this high diffusion coefficient of Ag, the formation of GPB region and consequently the formation of $Al_6(Cu,Ag)Mg_4$ precipitates are expected to increase in the coating sample containing 16.0 wt.% Ag. However, due to a decrease in the Ag content in the samples containing 5.3, and 10.6 wt.% Ag, there is a possibility of Ag being present elsewhere in the form of Ag-containing intermetallic such as $AlAg_2$, $AlAg_3$, and AgMg. The presence of precipitates and Ag-containing intermetallic in coated samples confirms the first reason mentioned earlier for the finer grain size in the coated samples containing Ag.

Figure 7 depicts the center zone microstructure of coating in the Ag-containing and Ag-free samples after homogenization and aging heat treatment. As shown in Fig. 7, after 4 h of homogenization and artificial aging, there was no significant difference in the microstructure of these samples. As can be observed in all of the coatings, grain growth occurred. The grain sizes of the coatings containing 0, 5.3, 10.6, and 16.0 wt.% Ag were (33.24±4.67), (32.29±2.86), (31.45±3.06) and (31.57±3.23) μm, respectively after heat treatment. Moreover, the microstructure of the substrate is shown in Fig. 7(e) after heat treatment. The grain sizes of the substrate before and after heat treatment were (45.10±3.20) and (83.33±9.83) μm, respectively. Most of the existing grain size non-uniformity is related to the substrate after heat treatment. In other words, abnormal grain growth in the substrate is more pronounced in comparison with the microstructure of the coatings. This may be due to a larger grain size of the substrate compared to that of the coatings.

According to the XRD results shown in Fig. 8, applying heat treatment in Ag-free samples had little to no effect on the nature of the precipitates and intermetallic. Meanwhile, after 4 h of homogenization and aging heat treatment applied to

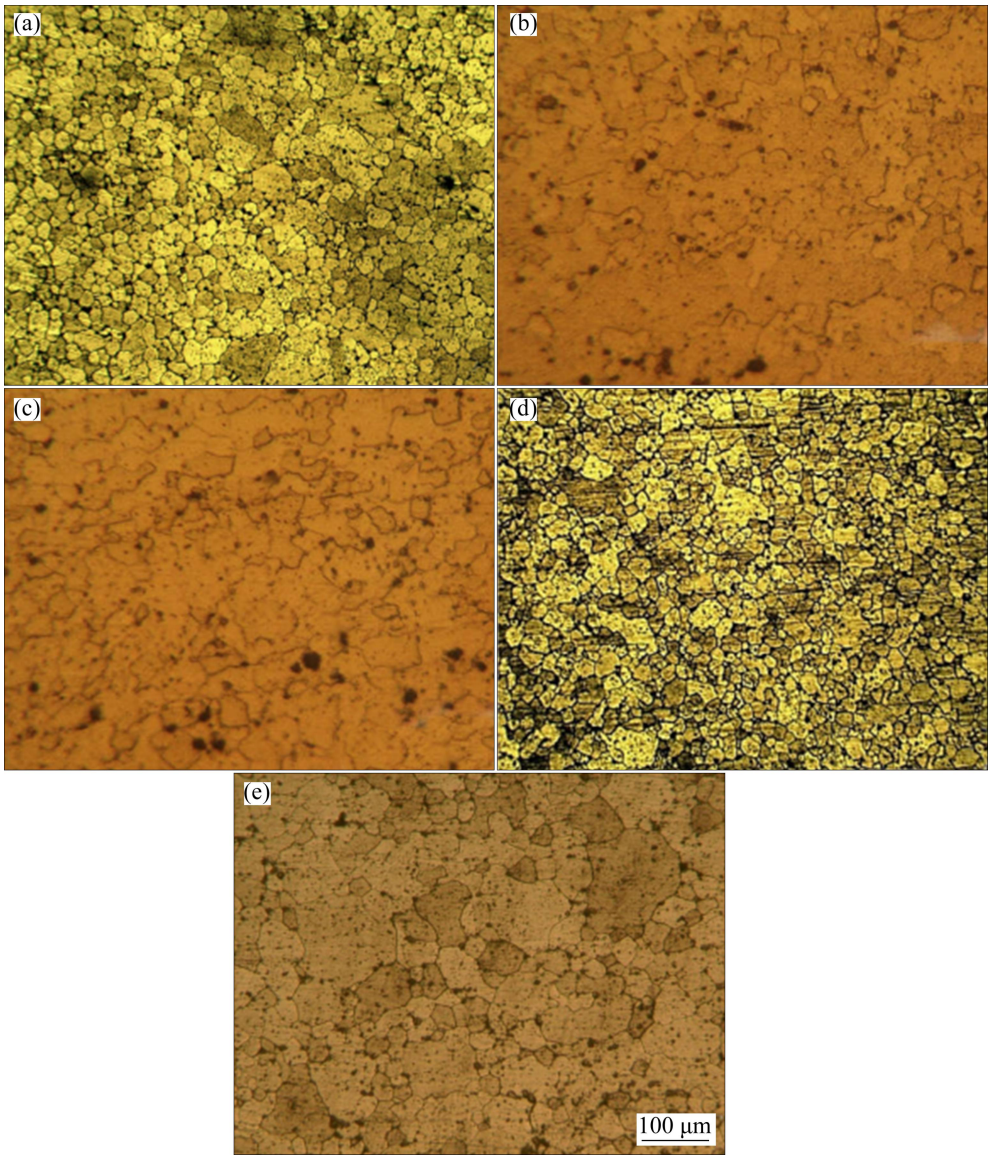

Fig. 7 Optical microscopy images at center of coated samples after homogenization and aging heat treatment for 4 h: (a) 0 wt.% Ag; (b) 5.3 wt.% Ag; (c) 10.6 wt.% Ag; (d) 16 wt.% Ag; (e) AA2024 substrate

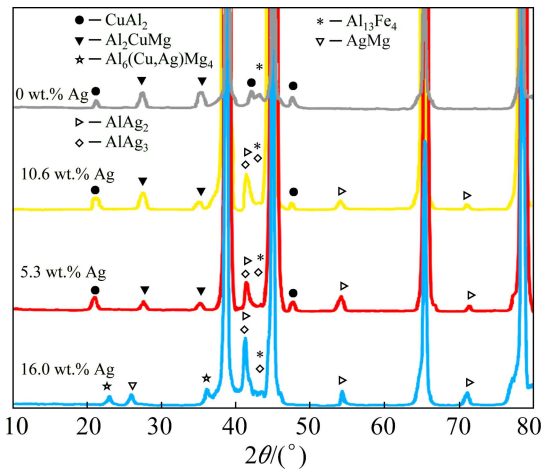

Fig. 8 XRD patterns of coated samples after heat treatment

the 16.0 wt.% Ag-containing sample, the peaks of Al_2CuMg and $CuAl_2$ precipitates disappeared. As one may observe, samples with 5.3 and 10.6 wt.% Ag do not possess $Al_6(Cu,Ag)Mg_4$ precipitates in their microstructures. However, Ag-rich intermetallics such as $AlAg_3$, $AlAg_2$, and AgMg were formed in their microstructures. It should also be noted that as the Ag content increased, the peak intensity of the Ag-rich particles expanded as well. As in the case with the Ag-free sample, the two samples with lower amounts of Ag (5.3 and 10.6 wt.% Ag), Al_2CuMg and $CuAl_2$ precipitates were formed in the microstructures after heat treatment. Nevertheless, due to the absence of $Al_6(Cu,Ag)Mg_4$ precipitates in these two coatings, it

is expected that the same level of hardness and strength present in the sample coated with 16.0 wt.% Ag may not be achieved.

For a more precise examination of the particles and precipitates formed in the microstructures of the coated samples, SEM images of all coated samples before and after the heat treatment are shown in Figs. 9 and 10, respectively. In the

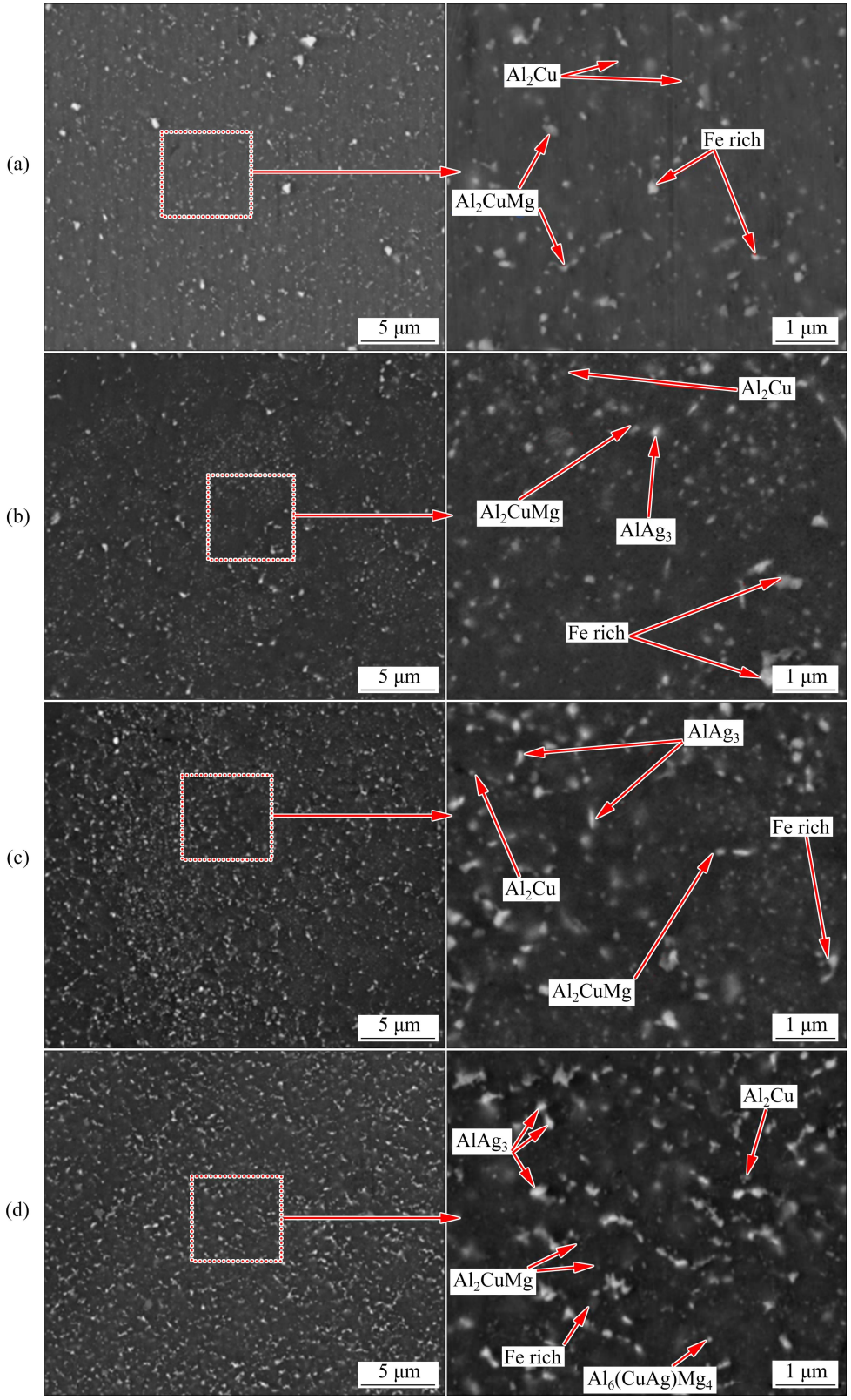

Fig. 9 SEM images of coated samples with different contents of Ag before heat treatment: (a) 0 wt.% Ag; (b) 5.3 wt.% Ag; (c) 10.6 wt.% Ag; (d) 16.0 wt.% Ag

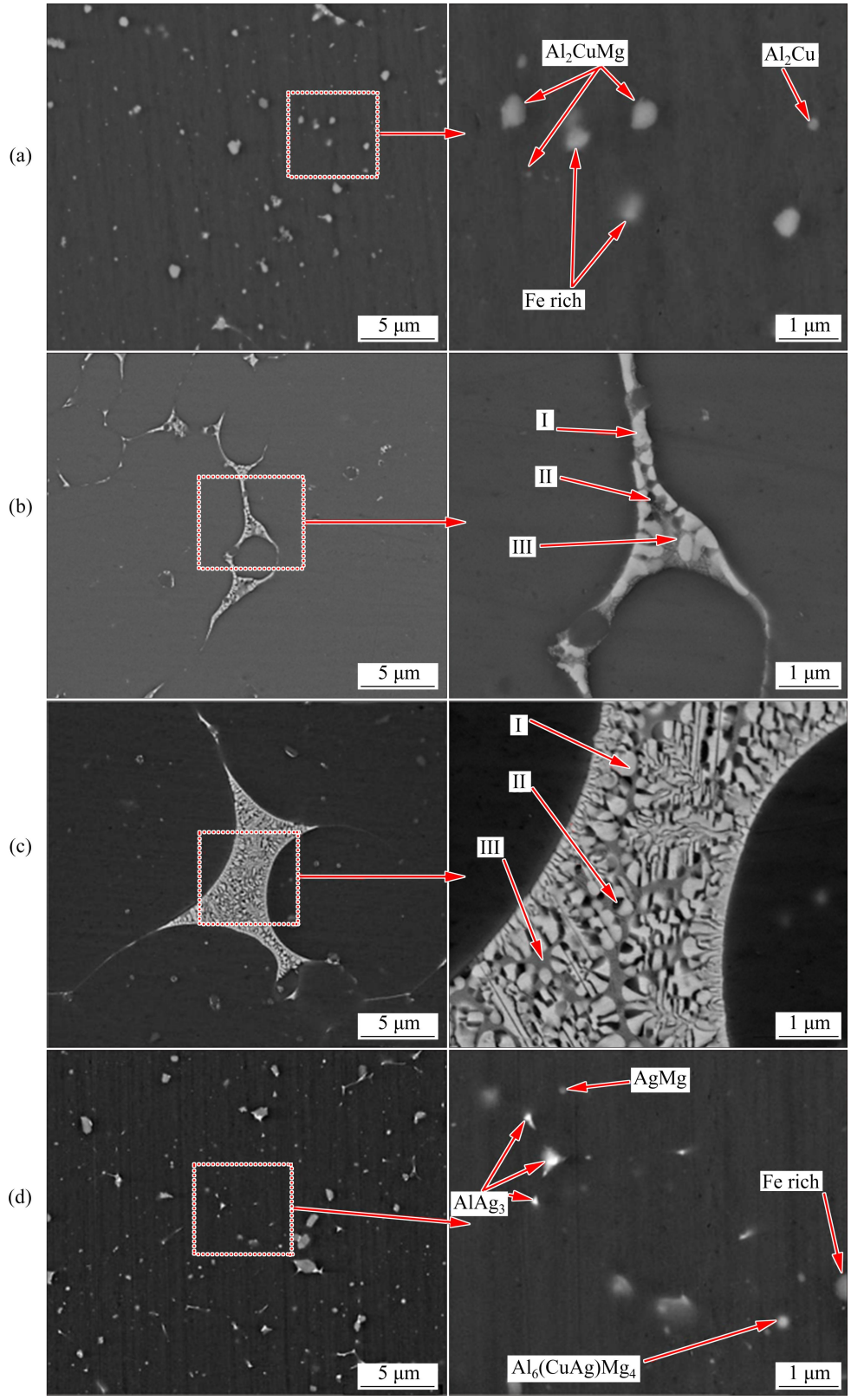

Fig. 10 SEM images of coated samples with different contents of Ag after heat treatment: (a) 0 wt.% Ag; (b) 5.3 wt.% Ag; (c) 10.6 wt.% Ag; (d) 16.0 wt.% Ag

Ag-containing and Ag-free samples, a high number of particles and precipitates, larger than 500 nm, are observed in the pre-heat treatment conditions (Fig. 9). The recognizable difference between the sample containing Ag and the one without Ag is the presence of a high content of Ag-rich particles

including $AlAg_2$, $AlAg_3$, and AgMg alongside a small amount of $Al_6(Cu,Ag)Mg_4$ precipitates in the 16.0 wt.% Ag sample. Furthermore, homogenization and aging of the Ag-free sample result in the formation of Al_2CuMg precipitates in the microstructure while the number of large precipitates and intermetallic may increase. Similarly, after homogenization and aging treatment for the Ag-containing samples, re-precipitation of strengthening precipitates occurs (Fig. 10). As is evident in the two samples containing 5.3 and 10.6 wt.% Ag, grain boundary is the region where the accumulation of particles and precipitates occurs. It should be noted that this process is not visible in all regions of the microstructure, but may appear in several areas of the coating. On the other hand, the microstructure of the sample coated with 16.0 wt.% Ag is quite uniform. Chemical analysis of particles and precipitates concentrated in the grain boundary has indicated that high contents of Cu and Mg accumulate alongside Ag in this region. This can be mainly due to the inhomogeneous distribution of Ag powder in several parts of the microstructure (as observed in the optical microscopy images) during heat treatment while the Ag-containing particles accumulate at high energy sites such as grain boundaries. Provided that there is no heterogeneous distribution of Ag powder in the microstructure, as is the case with 16.0 wt.% Ag, the particles and precipitates containing Ag should be evenly distributed in the microstructure after homogenization. The accumulation of Ag with Cu and Mg at grain boundaries has caused partial melting in a number of regions due to the homogenization temperature of 540 °C. The nature of the particles and the exact chemical formula of these particles observed in the grain boundary region cannot be accurately determined using EDS results for the samples with 5.3 and 10.6 wt.% Ag (Fig. 11). The mutual property of these two samples is the fact that the matrix of the grain boundary zone is full of Cu and Ag.

The hardness test results of the coatings before and after heat treatment are shown in Fig. 12(a). One can observe that with respect to the Ag-containing samples after coating before heat treatment, the hardness increases with a rise in the Ag content. The hardness values of the samples coated with 0, 5.3, 10.6, and 16.0 wt.% Ag were (84.87±1.58), (91.87±2.30), (95.38±2.20), and (96.06±2.70) BHN, respectively. Results obtained from the microstructure and X-ray diffraction analysis indicated that an increase in the coating hardness with a rise in the Ag content may be due to a smaller grain size, as well as formation and presence of Ag-containing precipitates and intermetallics such as $Al_6(Cu,Ag)Mg_4$, $AlAg_2$, $AlAg_3$, and AgMg.

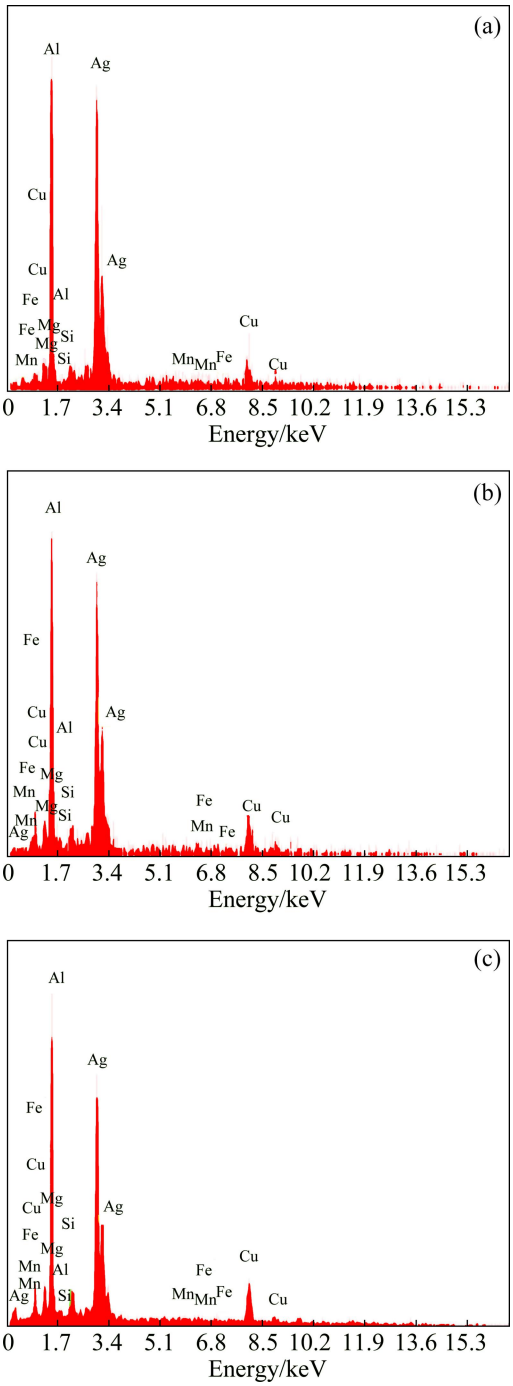

Fig. 11 EDS spectra of different zones in Fig. 10(b): (a) Spot I; (b) Spot II; (c) Spot III

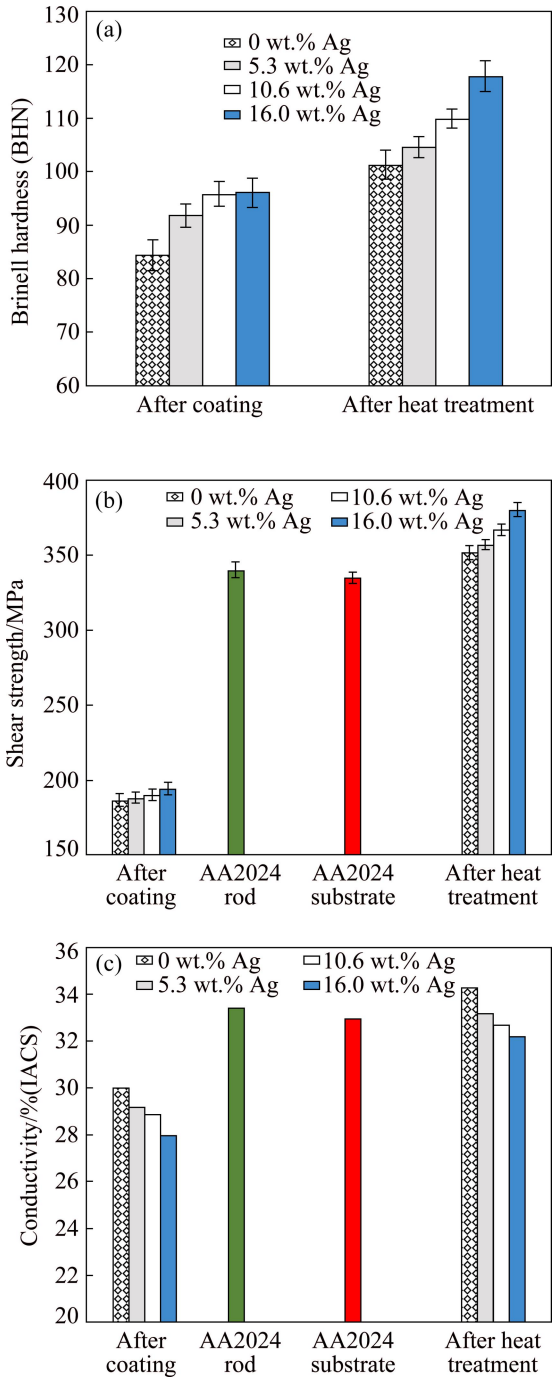

Fig. 12 Mechanical properties and electrical conductivity of coated samples: (a) Hardness; (b) Shear strength; (c) Electrical conductivity

As the Ag content increases, these particles are more likely to form and improve the coatings hardness. In addition, Ag present in the Al−Cu−Mg alloy forms the complex FCC phase of the $Al_6(Cu,Ag)Mg_4$ compared to the conventional formation of this phase by $CuAl_2$ and Al_2CuMg precipitates [39]. Moreover, the presence of Ag also increases the hardness and aging rate of Al−Cu−Mg alloys [7]. After heat treatment, the hardness values of the coated samples with 0, 5.3, 10.6, and 16.0 wt.% Ag were (101.34±1.05), (104.20±1.80), (110.00±1.90), and (117.88±2.80) BHN, separately. In the 16.0 wt.% Ag-coated sample, the presence of Ag-rich intermetallic compounds alongside with the $Al_6(Cu,Ag)Mg_4$ precipitates significantly increased the hardness compared to the 0, 5.3, and 10.6 wt.% Ag samples. Therefore, a higher value for hardness in the samples containing Ag, particularly in the samples with 10.6 and 16.0 wt.% Ag, confirms the effect of Ag on improving the aging and hardness of sample. On the other hand, the hardness of the coating with 5.3 wt.% Ag was close to that of the Ag-free sample. Therefore, one can propose that although Ag-rich intermetallic is formed in the 5.3 wt.% Ag sample, the slight improvement of hardness compared to the Ag-free sample indicates the low effect of Ag on its strength due its low content in the sample. Yet, another important point when comparing the 5.3 and 10.6 wt.% Ag samples with the 16.0 wt.% Ag sample is that the effect of $Al_6(Cu,Ag)Mg_4$ precipitates formation on strengthening is far greater than that of Ag-rich intermetallic. The shear strength of the coatings and consumable materials is illustrated in Fig. 12(b). Based on this figure, the shear strength trend is similar to the one observed in Fig. 12(a) for the hardness of samples. Before heat treatment the shear strengths of the samples coated with 0, 5.3, 10.6, and 16.0 wt.% Ag were (186.05±2.43), (188.01±2.52), (190.45±3.01), and (193.32±2.81) MPa, respectively. At this stage, the presence of smaller grains as well as Ag-containing particles and precipitates in addition to $CuAl_2$ and Al_2CuMg precipitates increases the overall strength of the coated samples containing Ag. However, after heat treatment, the shear strength of the samples coated with 0, 5.3, 10.6, and 16.0 wt.% Ag were (352.21±3.01), (357.78±2.79), (367.91±2.31), and (380.37±3.25) MPa, respectively. The high amount of $Al_6(Cu,Ag)Mg_4$ precipitates after aging can lead to a greater level of strength in the sample containing 16.0 wt.% Ag. Finally, the absence of $Al_6(Cu,Ag)Mg_4$ precipitates in the samples containing 5.3 and 10.6 wt.%, as well as the presence of partially melted structures in several grain boundary regions in these two samples can lead to a weaker coating and a decrease in their shear strengths.

The results for the electrical conductivity of the coatings before and after heat treatment, as well as the consumable rod and substrate are shown in Fig. 12(c). After friction surfacing, the electrical conductivity slightly decreases in the Ag-free sample compared to that of the substrate and rod. Moreover, due to the precipitation of fine particles and intermetallics formed during the coating and thus witnessing an increase in the interface between the particles and the matrix, as well as the probability of formation of the solid solution during friction surfacing, it can be expected that the electrical conductivity decreases. As one can observe, the sizes of particles and precipitates increase after the heat treatment while the contact area between the particles and matrix decreases, resulting in an overall increase in the electrical conductivity compared to the pre-heat treatment condition.

Therefore, as an important result, before and after heat treatment, the electrical conductivity is different for the samples containing Ag powder. Moreover, for the Ag-containing samples after the friction surfacing is carried out, the electrical conductivity decreases with an increase in the Ag content. Provided that a linear relationship is considered, one can propose that for every 1 wt.% increase in the Ag content, the electrical conductivity decreases by 0.12% (IACS). This electrical conductivity reduction is due to the formation of Al−Ag solid solution, as well as the presence of fine Ag-rich intermetallic in the microstructure of coatings before the heat treatment. The electrical conductivity increases after the heat treatment while decreases with an increase in the Ag content (the electrical conductivity decreases by 0.13% (IACS) with each addition of 1 wt.% Ag). As a result of heat treatment, a large amount of Ag exists in the solid solution form and appears as Ag-rich intermetallic compounds or coarse precipitates. Furthermore, by increasing the size of particles and precipitates and decreasing the contact area between the particles and aluminum matrix, their destructive effect on electrical conductivity decreases. It can be noticed that after heat treatment, the electrical conductivity of the samples containing 0 and 16.0 wt.% Ag were increased by 4.15% (IACS) and decreased by 2.15% (IACS), respectively.

4 Conclusions

(1) Adding small amount of Ag powder reduces the coating efficiency during the friction surfacing of AA2024 aluminum alloy. For instance, by adding 16.0 wt.% Ag, the coating efficiency is decreased from 20.01% to 18.85%.

(2) The formation of Al−Ag solid solution and intermetallic containing Ag, as well as lower heat input in the Ag-containing coatings can reduce the grain size of these coatings.

(3) Due to the high diffusion coefficient of Ag, the formation of GPB regions and consequently the formation of $Al_6(Cu,Ag)Mg_4$ precipitates in the sample containing 16.0 wt.% Ag is expected to increase.

(4) Heat treatment in the Ag-free sample has little to no effect on the nature of the precipitates and intermetallics. Meanwhile, after 4 h of homogenization and aging heat treatment, the 5.3 and 10.6 wt.% Ag samples do not possess $Al_6(Cu,Ag)Mg_4$ precipitates in their micro-structures.

(5) Homogenization and aging heat treatment of the Ag-free sample results in the formation of Al_2CuMg precipitates in its microstructure. Similarly, in Ag-containing samples, after homogenization and aging heat treatment, re-precipitation of strengthening precipitates occurs.

(6) The presence of Ag-rich intermetallic compounds along with the $Al_6(Cu,Ag)Mg_4$ precipitates in the 16.0 wt.% Ag coated sample significantly increases the hardness and strength of this sample compared to the other samples used in this study.

(7) Provided that a linear relationship is considered, it can be inferred that for every 1 wt.% increase in the Ag content, the electrical conductivity decreases by 0.12% (IACS).

Acknowledgments

The authors acknowledge the funding support of Babol Noshirvani University of Technology, Iran, through Grant Program No. BNUT/370167/99.

References

[1] MURASHKIN M Y, SABIROV I, SAUVAGE X, VALIEV R. Nanostructured Al and Cu alloys with superior strength and electrical conductivity [J]. Journal of Materials Science,

2016, 51(1): 33−49.

[2] MURASHKIN M, MEDVEDEV A, KAZYKHANOV V, KROKHIN A, RAAB G, ENIKEEV N, VALIEV R Z. Enhanced mechanical properties and electrical conductivity in ultrafine-grained Al 6101 alloy processed via ECAP-conform [J]. Metals, 2015, 5(4): 2148−2164.

[3] GAZIZOV M, KAIBYSHEV R. High cyclic fatigue performance of Al−Cu−Mg−Ag alloy under T6 and T840 conditions [J]. Transactions of Nonferrous Metals Society of China, 2017, 27(6): 1215−1223.

[4] XIA Q K, LIU Z Y, LI Y T. Microstructure and properties of Al−Cu−Mg−Ag alloy exposed at 200 °C with and without stress [J]. Transactions of Nonferrous Metals Society of China, 2008, 18(4): 789−794.

[5] HOU Y H, GU Y X, LIU Z Y, LI Y T, XU C. Modeling of whole process of ageing precipitation and strengthening in Al−Cu−Mg−Ag alloys with high Cu-to-Mg mass ratio [J]. Transactions of Nonferrous Metals Society of China, 2010, 20(5): 863−869.

[6] XIAO D H, HUANG B Y. Effect of Yb addition on precipitation and microstructure of Al−Cu−Mg−Ag alloys [J]. Transactions of Nonferrous Metals Society of China, 2007, 17(6): 1181−1185.

[7] AULD J, VIETZ J, POLMEAR I. *T*-phase precipitation induced by the addition of silver to an aluminium–copper–magnesium alloy [J]. Nature, 1966, 209(5024): 703−704.

[8] POLMEAR I. The influence of small additions of silver on the structure and properties of aged aluminum alloys [J]. JOM, 1968, 20(6): 44−51.

[9] SEN N, WEST D. The influence of 0.5 wt.% Ag on defect structures in an Al/3.2wt.%Cu/1.5wt.%Mg alloy [J]. Journal of Materials Science, 1968, 3(3): 266−270.

[10] SEN N, WEST D. Some factors influencing *S* precipitation in Al−Cu−Mg and Al−Cu−Mg−Ag alloys [J]. Journal of the Institute of Metals, 1969, 97: 87−92.

[11] NIKULIN I, KIPELOVA A, GAZIZOV M, TELESHOV V, ZAKHAROV V, KAIBYSHEV R. Novel Al−Cu−Mg−Ag alloy for high temperature applications [C]//Proceedings of the 12th ICAA. Tokyo: The Japan Institute of Light Metals, 2010: 2303−2308.

[12] TOLAMINEJAD B, ATHAR M H, ARABI H, TAHERI A K. Enhanced grain refinement of commercial pure copper using the ECAE of Al−Cu−Al tri-layer composite [J]. Engineering Science and Technology: An International Journal, 2016, 19(1): 254−259.

[13] CHEN S Y, CHANG G W, YUE X D, LI Q C. Solidification process and microstructure of transition layer of Cu−Al composite cast prepared by method of pouring molten aluminum [J]. Transactions of Nonferrous Metals Society of China, 2016, 26(8): 2247−2256.

[14] SAPANATHAN T, KHODDAM S, ZAHIRI S H. Spiral extrusion of aluminum/copper composite for future manufacturing of hybrid rods: A study of bond strength and interfacial characteristics [J]. Journal of Alloys and Compounds, 2013, 571: 85−92.

[15] KIM I K, HONG S I. Mechanochemical joining in cold roll-cladding of tri-layered Cu/Al/Cu composite and the interface cracking behavior [J]. Materials & Design, 2014, 57: 625−631.

[16] KIM I K, HONG S I. Effect of heat treatment on the bending behavior of tri-layered Cu/Al/Cu composite plates [J]. Materials & Design, 2013, 47: 590−598.

[17] GLADKOVSKY S, KUTENEVA S, SERGEEV S. Microstructure and mechanical properties of sandwich copper/steel composites produced by explosive welding [J]. Materials Characterization, 2019, 154: 294−303.

[18] LIN W, DU Q L, CHANG L, CUI X H, XING Z, YU H L. Enhanced mechanical properties of lamellar Cu/Al composites processed via high-temperature accumulative roll bonding [J]. Transactions of Nonferrous Metals Society of China, 2019, 29(8): 1621−1630.

[19] DI C, ZHANG J Y, YAO J J, HAN Y Q, WU C J. Cu–Al interfacial compounds and formation mechanism of copper cladding aluminum composites [J]. Transactions of Nonferrous Metals Society of China, 2017, 27(11): 2521−2528.

[20] ANSARIAN I, SHAERI M. Diffusional bonds in laminated composites produced by ECAP [J]. Transactions of Nonferrous Metals Society of China, 2017, 27(9): 1928−1938.

[21] GANDRA J, KROHN H, MIRANDA R, VILAÇA P, QUINTINO L, DOS SANTOS J. Friction surfacing—A review [J]. Journal of Materials Processing Technology, 2014, 214(5): 1062−1093.

[22] ESTHER I, DINAHARAN I, MURUGAN N. Microstructure and wear characterization of AA2124/4wt.%B_4C nano-composite coating on Ti−6Al−4V alloy using friction surfacing [J]. Transactions of Nonferrous Metals Society of China, 2019, 29(6): 1263−1274.

[23] KORMOUT K S, PIPPAN R, BACHMAIER A. Deformation-induced supersaturation in immiscible material systems during high-pressure torsion [J]. Advanced Engineering Materials, 2017, 19(4): 1600675.

[24] BACHMAIER A, SCHMAUCH J, ABOULFADL H, VERCH A, MOTZ C. On the process of co-deformation and phase dissolution in a hard-soft immiscible CuCo alloy system during high-pressure torsion deformation [J]. Acta Materialia, 2016, 115: 333−346.

[25] NIE J, LIU M, WANG F, ZHAO Y, LI Y, CAO Y, ZHU Y T. Fabrication of Al/Mg/Al composites via accumulative roll bonding and their mechanical properties [J]. Materials, 2016, 9(11): 1−14.

[26] YADAV D, BAURI R, CHAWAKE N. Fabrication of Al−Zn solid solution via friction stir processing [J]. Materials Characterization, 2018, 136: 221−228.

[27] PIRHAYATI P, JAMSHIDI AVAL H. Effect of silver on non-isothermal aging of friction surfaced AA2024−16wt.% Ag composites [J]. Surface and Coatings Technology, 2019, 379: 125059.

[28] DILIP J, BABU S, RAJAN S V, RAFI K, RAM G J, STUCKER B. Use of friction surfacing for additive manufacturing [J]. Materials and Manufacturing Processes, 2013, 28(2): 189−194.

[29] SHEN J, HANKE S, ROOS A, SANTOS J F D, KLUSEMANN B. Fundamental study on additive manufacturing of aluminum alloys by friction surfacing layer deposition [C]//AIP Conference Proceedings. AIP Publishing LLC, 2019, 2113(1): 150015.

[30] KHODABAKHSHI F, GERLICH A. Potentials and strategies of solid-state additive friction-stir manufacturing technology: A critical review [J]. Journal of Manufacturing Processes, 2018, 36: 77−92.
[31] LUCAS G, ODETTE G, SHECKHERD J. STP888: Shear punch and microhardness tests for strength and ductility measurements: The use of small-scale specimens for testing irradiated material [S]. ASTM International, 1986.
[32] SUHUDDIN U, MIRONOV S, KROHN H, BEYER M, DOS SANTOS J. Microstructural evolution during friction surfacing of dissimilar aluminum alloys [J]. Metallurgical and Materials Transactions A, 2012, 43(13): 5224−5231.
[33] MUZYK M, PAKIEŁA Z, KURZYDŁOWSKI K J. Generalized stacking fault energies of aluminum alloys — Density functional theory calculations [J]. Metals, 2018, 8(10): 1−9.
[34] RUSSELL A, LEE K L. Structure-property relations in nonferrous metals [M]. Hoboken, New Jersey: John Wiley & Sons, 2005.
[35] BARARPOUR S M, JAMSHIDI AVAL H, JAMAATI R. Modeling and experimental investigation on friction surfacing of aluminum alloys [J]. Journal of Alloys and Compounds, 2019, 805: 57−68.
[36] PIRHAYATI P, JAMSHIDI AVAL H. An investigation on thermo-mechanical and microstructural issues in friction surfacing of Al−Cu aluminum alloys [J]. Materials Research Express, 2019, 6(5): 056550.
[37] NELSON J B, RILEY D. An experimental investigation of extrapolation methods in the derivation of accurate unit-cell dimensions of crystals [J]. Proceedings of the Physical Society, 1945, 57(3): 160−177.
[38] MEHRER H. Diffusion in solid metals and alloys [M]. Heidelberg: Springer−Verlag, 1990.
[39] TAYLOR J, PARKER B, POLMEAR I. Precipitation in Al−Cu−Mg−Ag casting alloy [J]. Metal Science, 1978, 12(10): 478−482.

摩擦堆焊 AA2024−Ag 复合材料的显微组织表征与力学性能

Parisa PIRHAYATI, Hamed JAMSHIDI AVAL

Department of Materials Engineering, Babol Noshirvani University of Technology,
Shariati Avenue, Babol 47148-71167, Iran

摘　要：研究银对摩擦堆焊 AA2024 铝合金涂层显微组织、力学性能和电导率的影响。银添加方式为先在 AA2024 铝合金耗材棒横截表面钻孔，再在孔内填充银粉，其添加量为 5.3、10.6 和 16.0%(质量分数)。结果表明，固溶强化、析出相和含银金属间化合物的形成降低晶粒生长的驱动力，从而降低涂层中的晶粒尺寸。经人工时效热处理后，含 0% Ag(质量分数)涂层的电导率提高了 4.15%(IACS)，而含 16.0% Ag(质量分数)涂层的电导率降低 2.15%(IACS)。当考虑线性关系时，在银含量 Ag 增加 1%(质量分数)的条件下，涂层的强度和硬度分别增加 1.8%和 1.0%。$Al_6(Cu,Ag)Mg_4$ 析出相的形成比富 Ag 金属间化合物的形成对强化的影响更大。

关键词：摩擦堆焊；AA2024 铝合金；银粉；AA2024−Ag 复合材料

(Edited by Wei-ping CHEN)